

Calculation of Penetration Depth and T_c in κ -(ET) $_2$ Cu(NCS) $_2$ under Pressure

Kazunori TANAKA *, Hiroaki IKEDA and Kosaku YAMADA

Department of science, Kyoto university, Kyoto 606-8502, Japan

(Received July 7, 2004)

The pressure dependence of the inverse square of the magnetic penetration depth λ^{-2} in κ -(ET) $_2$ Cu(NCS) $_2$ was measured by Larkin, *et al.* According to the paper, λ^{-2} behaves differently under low pressure and under high pressure. Under low pressure, the development of λ^{-2} just below $T = T_c$ is rapid compared to the case under high pressure. Moreover, T_c in κ -(ET) $_2$ Cu(NCS) $_2$ increases under c -axis pressure up to 1kbar and decreases under higher pressure, while T_c decreases monotonically under the hydrostatic pressure, or under the uniaxial pressure parallel to other axes. In order to explain these behaviors, we calculate T_c and λ^{-2} for κ -(ET) $_2$ Cu(NCS) $_2$ under pressure. In the calculation we mainly use an effective dimer Hubbard model. In conclusion, the behavior of λ^{-2} results from three effects: the variation of the bandwidth of quasiparticles, the change of the Fermi surfaces, and the effect of vertex correction. This is a different mechanism from that of λ^{-2} in cuprates which we observe when the doping varies. Moreover, we explain the increase in T_c under the c -axis pressure up to 1kbar and the decrease in T_c over 1kbar from our calculation. With the increase in the c -axis pressure, two competitive effects with respect to T_c appear. One is the approach of the Fermi surface to the antiferromagnetic Brillouin zone boundary, and the other is the suppression of the electron correlation. Under the low c -axis pressure, T_c increases since the former effect is dominant. On the other hand, T_c decreases since the latter effect is dominant under the high c -axis pressure.

KEYWORDS: unconventional superconductivity, organic superconductor, penetration depth, vertex correction, pressure

1. Introduction

Recently, many measurements have been performed in the superconducting state in organic conductors including κ -(ET) $_2$ Cu(NCS) $_2$. Many interesting behaviors are observed under pressure in organic conductors, since they are soft materials. Among them, we study the pressure dependence of the inverse square of the magnetic penetration depth λ^{-2} and the behavior of the superconducting transition temperature T_c under the hydrostatic and the uniaxial pressure by using the effective dimer Hubbard model.

We calculate λ^{-2} in κ -(ET) $_2$ Cu(NCS) $_2$ on the basis of Jujo's theory.^{1,2} This theory is a general theory on the transport phenomena and the magnetic penetration depth in the

*E-mail address: tanaka.kazunori@scphys.kyoto-u.ac.jp

superconducting state, including the effect of the vertex correction, and can be applied to unconventional superconductors such as cuprates and organic superconductors κ -(ET)₂X. By taking account of the vertex correction, which can be considered as the backflow effect, this theory explains why the value of inverse square of the magnetic penetration depth λ^{-2} is suppressed near $T = 0$ under the strong antiferromagnetic fluctuation in unconventional superconductors, such as cuprates in the underdoped region. In this paper we discuss the pressure dependence of the extrapolated value of λ^{-2} at $T = 0$ and the development of λ^{-2} just below T_c . Moreover, T_c under pressure is calculated by the linearized Dyson-Gor'kov equations, and the different dependence of T_c on hydrostatic and uniaxial pressure is explained.

2. The Pressure Dependence of λ^{-2} and of T_c in κ -(ET)₂Cu(NCS)₂

The pressure dependence of the inverse square of the magnetic penetration depth λ^{-2} in κ -(d₈ET)₂Cu(NCS)₂ was measured by Larkin, *et al.*³ Here, we refer to κ -(ET)₂Cu(NCS)₂ in which hydrogens in ET molecules are deuterated as κ -(d₈ET)₂Cu(NCS)₂, while the materials with protonated ones are referred to as κ -(h₈ET)₂Cu(NCS)₂. Ref.3 shows that the value of $\left. \frac{d\lambda^{-2}}{dT} \right|_{T=T_c}$ is large under low pressure ($P = 0$ bar) compared to that under high pressure (P is up to 1290 bar). This implies that there is a rapid development of λ^{-2} just below T_c under low pressure. Moreover, Ref.3 shows that λ^{-2} is suppressed in the low temperature region under low pressure, although the data near $T = 0$ is insufficient. This suppression is analogous to the doping dependence of λ^{-2} in high- T_c cuprates such as LSCO.⁴ The λ^{-2} - T diagram in the underdoped and overdoped LSCO behaves similarly to κ -(ET)₂Cu(NCS)₂ under low pressure and under high pressure, respectively. The behavior of λ^{-2} in cuprates is understood from the fact that the effect of the vertex correction is strong in the underdoped region, and weak in the overdoped region. The vertex correction affects strongly under low pressure and weakly under high pressure in κ -(ET)₂Cu(NCS)₂. In this paper, we study the behavior of λ^{-2} in κ -(ET)₂Cu(NCS)₂ theoretically by carrying out the actual calculation.

Next, we refer to the pressure dependence of T_c for κ -(ET)₂Cu(NCS)₂. T_c under the hydrostatic pressure have been measured by many experiments.⁵⁻⁷ According to the results, T_c decreases monotonically as the pressure increases. On the other hand, the behavior of T_c under the uniaxial pressure is quite different from that under the hydrostatic pressure according to the recent measurements for κ -(ET)₂Cu(NCS)₂.⁸⁻¹⁰ When the uniaxial pressure is applied in parallel to b -axis or to a -axis, T_c decreases. This is similar to the behavior under the hydrostatic pressure. On the other hand, T_c increases up to 1kbar under the c -axis pressure and decreases under higher pressure, which is in contrast to the behavior of T_c under the hydrostatic pressure. By calculation, we show that this is because two competitive effects with respect to T_c appear under the c -axis pressure: the approach of the Fermi surface to the antiferromagnetic Brillouin zone boundary and the suppression of the electron correlation.

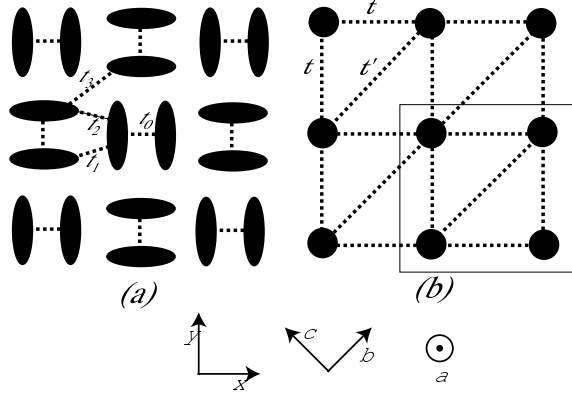


Fig. 1. (a): The original lattice structure of κ -(ET) $_2$ X, where the ellipses represent ET molecules. A dimer consists of two parallel ET molecules. (b): The lattice structure of κ -(ET) $_2$ X when the pair of ET molecules are dimerized.^{11,12} The circles represent dimers, and the rectangle represents the unit cell. κ -(ET) $_2$ X is quasi-two-dimensional (Q2D) conductor where the layer is usually denoted as the bc -plane. x - and y -axes are introduced for the convenience of calculation. a -axis is perpendicular to the bc -plane.

3. Effective Dimer Hubbard model for Organic Superconductor κ -(ET) $_2$ X

We use the effective dimer Hubbard model for κ -(ET) $_2$ X.^{5,6,11,12} In this paper we adopt a quasi-two-dimensional (Q2D) band structure ignoring the interlayer hopping term for κ -(ET) $_2$ X and symmetrize two dimers in the unit cell.⁶ Then the Hamiltonian is expressed as follows:¹³

$$H = \sum_{\mathbf{k}} \varepsilon_{\mathbf{k}} c_{\mathbf{k}\sigma}^\dagger c_{\mathbf{k}\sigma} + U \sum_{\mathbf{k}, \mathbf{k}', \mathbf{q}} c_{\mathbf{k}\uparrow}^\dagger c_{\mathbf{q}-\mathbf{k}\downarrow}^\dagger c_{\mathbf{q}-\mathbf{k}'\downarrow} c_{\mathbf{k}'\uparrow}, \quad (1)$$

$$\varepsilon_{\mathbf{k}} = -2t(\cos k_x + \cos k_y) - 2t' \cos(k_x + k_y), \quad (2)$$

where t and t' are the nearest-neighbor and next-nearest-neighbor hopping terms shown in Fig.1. U is the Coulomb repulsion and $\varepsilon_{\mathbf{k}}$ is the dispersion. The bandwidth W is expressed as the maximum of the dispersion measured from the minimum: $\varepsilon_{\mathbf{k}max} - \varepsilon_{\mathbf{k}min} \sim 8t$. The exact value of W is $8.22t$ and $8.39t$ at $t'/t = 0.7$ and 0.75 , respectively. In κ -(ET) $_2$ X, the electrons are half-filled. In this paper, we adopt the FLEX approximation, the self-consistent second order perturbation theory (SC-SOPT), and the third order perturbation theory (TOPT) in the calculation of the self-energy terms.^{1,2} We adopt different approximations in the calculation for λ^{-2} and for T_c . In the calculation for λ^{-2} FLEX and SC-SOPT are adopted, since conservation approximations are needed. FLEX is appropriate for the case with the strong antiferromagnetic fluctuation, while SC-SOPT is used to show the weak correlation effect and the weak antiferromagnetic fluctuation qualitatively. On the other hand, SC-SOPT is not enough to give actual T_c since the third order term in U is important for calculating T_c . Therefore when the antiferromagnetic fluctuation is weak, we adopt TOPT instead of SC-SOPT in

the calculation for T_c . As a conclusion, we adopt FLEX and TOPT in the calculation for T_c . The former is used for the strong antiferromagnetic fluctuation and the latter is used for the weak correlation.

Within FLEX and SC-SOPT, the self-energy term and the Green's function in the normal state Σ_n is expressed as follows:

$$\Sigma_n(k) = \frac{T}{N} \sum_q V(q) G(k-q), \quad (3)$$

$$G(k) = \frac{1}{i\varepsilon_n - (\varepsilon_{\mathbf{k}} - \mu) - \Sigma_n(k)}, \quad (4)$$

where $k = (\mathbf{k}, \varepsilon_n)$, $\varepsilon_n = (2n+1)\pi T$ is the fermion Matsubara frequency, and μ is the chemical potential. The normal vertex $V(q)$ in Eq.3 is given by

$$V(q) = \frac{3}{2}U^2 \frac{\chi(q)}{1 - U\chi(q)} + \frac{1}{2}U^2 \frac{\chi(q)}{1 + U\chi(q)} - U^2\chi(q) \quad (5)$$

for FLEX and

$$V(q) = U^2\chi(q) \quad (6)$$

for SC-SOPT. The spin susceptibility $\chi(q)$ is expressed as

$$\chi(q) = -\frac{T}{N} \sum_q G(k+q) G(k). \quad (7)$$

Note that $q = (\mathbf{q}, \omega_l)$, and $\omega_l = 2n\pi T$ is the boson Matsubara frequency. Within FLEX and SC-SOPT, we obtain the normal self-energy term and the normal Green's function by solving Eqs.3 and 4 self-consistently.

Within TOPT, the normal self-energy term is expressed as follows.

$$\Sigma_n(k) = \frac{T}{N} \sum_{k'} [U^2\chi_0(k-k') + U^3\chi_0^2(k-k') + U^3\phi_0^2(k+k')] G_0(k'), \quad (8)$$

$$\chi_0(q) = -\frac{T}{N} \sum_k G_0(k)G_0(k+q), \quad (9)$$

$$\phi_0(q) = -\frac{T}{N} \sum_k G_0(k)G_0(q-k), \quad (10)$$

where $\chi_0(q)$ and $\phi_0(q)$ are calculated from the bare Green's function $G_0(k) = \frac{1}{i\varepsilon_n - (\varepsilon_{\mathbf{k}} - \mu)}$ and $\chi_0(q) \neq \chi(q)$. This shows that the calculation of the self-energy term and the Green function within TOPT is not self-consistent in contrast to FLEX and SC-SOPT. This is because self-consistent TOPT seems to be complicated in actual calculation.

Here we introduce the FLEX approximation in the superconducting state, the normal and anomalous self-energy terms $\Sigma_n(k)$ and $\Sigma_a(k)$ are given by

$$\Sigma_n(k) = \frac{T}{N} \sum_q V_n(q) G(k-q), \quad (11)$$

$$\Sigma_a(k) = -\frac{T}{N} \sum_q V_a(q) F(k-q), \quad (12)$$

where $V_n(q)$ and $V_a(q)$ are the normal and anomalous vertices in the superconducting state, respectively. The normal and anomalous Green's functions $G(k-q)$ and $F(k-q)$ are written as

$$G(k) = \frac{i\varepsilon_n + (\varepsilon_{\mathbf{k}} - \mu) + \Sigma_n(-k)}{[i\varepsilon_n - (\varepsilon_{\mathbf{k}} - \mu) - \Sigma_n(k)][i\varepsilon_n + (\varepsilon_{\mathbf{k}} - \mu) + \Sigma_n(-k)] - \Sigma_a(k)^2}, \quad (13)$$

$$F(k) = \frac{-\Sigma_a(k)}{[i\varepsilon_n - (\varepsilon_{\mathbf{k}} - \mu) - \Sigma_n(k)][i\varepsilon_n + (\varepsilon_{\mathbf{k}} - \mu) + \Sigma_n(-k)] - \Sigma_a(k)^2}. \quad (14)$$

$V_n(q)$ and $V_a(q)$ are given by

$$V_n(q) = \frac{U^2}{2} \left[3 \frac{\chi_s(q)}{1 - U\chi_s(q)} - \chi_s(q) + \frac{\chi_c(q)}{1 + U\chi_c(q)} - \chi_c(q) \right], \quad (15)$$

$$V_a(q) = \frac{U^2}{2} \left[3 \frac{\chi_s(q)}{1 - U\chi_s(q)} - \chi_s(q) - \frac{\chi_c(q)}{1 + U\chi_c(q)} + \chi_c(q) \right], \quad (16)$$

with

$$\chi_c(q) = -\frac{T}{N} \sum_q [G(k+q)G(k) \pm F(k+q)F(k)], \quad (17)$$

where $+$ and $-$ correspond to χ_s and χ_c , respectively.

We solve Eqs.11-17 self-consistently to calculate $G(k)$, $F(k)$, $\Sigma_n(k)$ and $\Sigma_a(k)$. The symmetry of Cooper pair in κ -(ET)₂X is $d_{x^2-y^2}$, with which the superconducting gap $\Sigma_a(k)$ has nodes in $\pm\pi/4$ directions in the k -space.¹³ The $d_{x^2-y^2}$ gap symmetry for κ -(ET)₂X is justified later in calculating T_c . In order to realize this symmetry, we set $\Sigma_a(\mathbf{k}, \varepsilon_{\pm 1}) \propto (\cos k_x - \cos k_y)$ as the initial value for solving Eqs.11-17.

4. Calculation of T_c by Dyson-Gor'kov Equations

In this section, we calculate T_c in κ -(ET)₂X by the linearized Dyson-Gor'kov equation within FLEX¹⁴⁻¹⁸ and TOPT.¹³ First of all, the normal and anomalous Green's functions satisfy Dyson-Gor'kov equations.¹⁹

$$G(k) = G_0(k) + G_0(k) \Sigma_n(k) G(k) + G_0(k) \Sigma_a(k) F^\dagger(k), \quad (18)$$

$$F^\dagger(k) = G_0(-k) \Sigma_n(-k) F^\dagger(k) + G_0(-k) \Sigma_a(-k) G(k). \quad (19)$$

When T approaches T_c within the superconducting state, Eqs.18 and 19 are linearized as follows, since $F(k) \ll G(k)$.

$$F(k) = |G(k)|^2 \Sigma_a(k), \quad (20)$$

$$G(k) = G_0(k) + G_0(k) \Sigma_n(k) G(k). \quad (21)$$

Within FLEX, $\Sigma_n(k)$ and $\Sigma_a(k)$ in the vicinity of T_c are calculated by linearizing Eqs.11 and 12, respectively. Then, $\Sigma_n(k)$ is the same as that in the normal state, which is expressed by

Eqs.3 and 5, while $\Sigma_a(k)$ is expressed by the linearized Dyson-Gor'kov equation:

$$\Sigma_a(k) = -\frac{T}{N} \sum_{k'} V_a(q) |G(k-q)|^2 \Sigma_a(k-q), \quad (22)$$

$$V_a(q) = U^2 \left[\frac{3}{2} \frac{\chi(q)}{1-\chi(q)} - \frac{1}{2} \frac{\chi(q)}{1+\chi(q)} \right] + U. \quad (23)$$

On the other hand, the linearized Dyson-Gor'kov equation for TOPT is

$$\Sigma_a(k) = -\frac{T}{N} \sum_{k'} V_a(k, k') |G(k')|^2 \Sigma_a(k'), \quad (24)$$

where,

$$V_a(k, k') = V_{RPA}(k, k') + V_{vert}(k, k'), \quad (25)$$

$$V_{RPA}(k, k') = U + U^2 \chi_0(k+k') + 2U^3 \chi_0^2(k+k'), \quad (26)$$

$$V_{vert}(k, k') = 2U^3 \frac{T}{N} \text{Re} \sum_{k_1} G_0(k_1) G_0(k+k_1-k') [\chi_0(k+k_1) - \phi_0(k+k_1)]. \quad (27)$$

If we replace the left hand side of Eqs.22 and 24 by $\alpha \Sigma_a(k)$, this equation can be considered as an eigenvalue equation with eigenvalue α and eigenvector $\Sigma_a(k)$. T_c is the temperature at which the maximum eigenvalue α_{max} reaches to unity. $\Sigma_a(k)$ with which the largest eigenvalue is obtained represents the superconducting gap symmetry. Among several gap functions, the $d_{x^2-y^2}$ state possesses the maximum eigenvalue in the region $0.17 < t/U < 0.35$ and $0.4 < t'/t < 0.8$ within FLEX, and $0.14 < t/U < 0.25$ and $0.4 < t'/t < 0.8$ within TOPT.

5. Effect of the vertex correction and λ^{-2} : Introduction to Jujo's theory.

In this section, we introduce Jujo's theory shortly. From Kubo formula, the penetration depth is expressed with the electromagnetic response kernel as follows.

$$\lambda_{\mu\nu}^{-2} = -4\pi K_{\mu\nu}(q \rightarrow 0), \quad (28)$$

$$K_{\mu\nu}(q \rightarrow 0) = -\frac{T}{N} \sum_{\mathbf{k}, n} \text{Tr} \left[\hat{\Lambda}_\mu^0(k, k+q) \hat{G}(k+q) \hat{\Lambda}_\nu(k+q, k) \hat{G}(k) \right]_{q \rightarrow 0} - \frac{T}{V} \sum_{\mathbf{k}, n} \frac{\partial^2 \varepsilon_{\mathbf{k}}}{\partial k_\nu \partial k_\mu} \text{Tr} \left[\hat{\tau}_3 \hat{G}(k) \right] e^{i\varepsilon_n 0+}. \quad (29)$$

Equation 29 is expressed by Nambu matrices. The Green's function matrix is defined as:

$$\begin{aligned} \hat{G}(k) &= \begin{pmatrix} G(k) & F(k) \\ F(k) & -G(-k) \end{pmatrix} \\ &= \frac{1}{i\varepsilon_n \hat{\tau}_0 - \varepsilon_{\mathbf{k}} \hat{\tau}_3 - \hat{\Sigma}(k)}, \end{aligned} \quad (30)$$

where the self-energy matrix $\hat{\Sigma}(k)$ is given by

$$\hat{\Sigma}(k) = \begin{pmatrix} \Sigma_n(k) & \Sigma_a(k) \\ \Sigma_a(k) & -\Sigma_n(-k) \end{pmatrix}. \quad (31)$$

Matrices $\hat{\tau}_0$ and $\hat{\tau}_3$ are given by

$$\hat{\tau}_0 = \begin{pmatrix} 1 & 0 \\ 0 & 1 \end{pmatrix}, \quad (32)$$

$$\hat{\tau}_3 = \begin{pmatrix} 1 & 0 \\ 0 & -1 \end{pmatrix}. \quad (33)$$

$$\hat{\Lambda}_\mu^0(k, k+q) \Big|_{q \rightarrow 0} = \begin{pmatrix} v_{\mathbf{k}\mu} & 0 \\ 0 & v_{\mathbf{k}\mu} \end{pmatrix} \quad (34)$$

is the bare three-point vertex, where $v_{\mathbf{k}} = \frac{\partial \varepsilon_{\mathbf{k}}}{\partial \mathbf{k}}$ is the bare velocity of electrons. $\hat{\Lambda}_\mu(k+q, k)$ satisfy the following integral equation:

$$\begin{aligned} \hat{\Lambda}_{\mu ij}(k+q, k) &= \hat{\Lambda}_{\mu ij}^0(k+q, k) \\ &+ \frac{T}{N} \sum_{k'} \sum_{m,n} \Gamma_{in,mj}(k+q, k'; k'+q, k) \left(\hat{G}(k'+q) \hat{\Lambda}_\mu(k'+q, k') \hat{G}(k') \right)_{m,n}, \end{aligned} \quad (35)$$

where irreducible four-point vertex $\Gamma_{in,mj}$ is expressed by the functional derivative of the self-energy matrix by the Green's function matrix:

$$\Gamma_{in,mj} = \frac{\delta \Sigma_{ij}[\hat{G}]}{\delta G_{mn}}. \quad (36)$$

After rather long calculation shown in Refs.1 and 2, Eq.28 is rewritten as

$$\lambda_{\mu\nu}^{-2} = 8\pi \int_{FS} \frac{dS_{\mathbf{k}'}}{(2\pi)^3 |v_{\mathbf{k}'}^*|} v_{\mathbf{k}'\mu}^* (1 - Y(\mathbf{k}'; T)) \bar{v}_{\mathbf{k}'\nu}^*, \quad (37)$$

where $\bar{v}_{\mathbf{k}}^*$ is the renormalized velocity of quasiparticles in the superconducting state. See Ref.1 for the detailed calculation of $\bar{v}_{\mathbf{k}}^*$. $Y(\mathbf{k}; T)$ is Yosida function:

$$Y(\mathbf{k}; T) = - \int d\varepsilon_{\mathbf{k}}^* \left(\frac{\partial f(E_{\mathbf{k}})}{\partial E_{\mathbf{k}}} \right). \quad (38)$$

In Eq.38, $f(x) = (e^{x/T} + 1)^{-1}$ is the Fermi distribution function and $E_{\mathbf{k}} = \sqrt{\varepsilon_{\mathbf{k}}^{*2} + (\Delta_{\mathbf{k}}^*)^2}$, where $\Delta_{\mathbf{k}}^* = z_{\mathbf{k}} \Delta_{\mathbf{k}}$ is the renormalized superconducting gap. $\Delta_{\mathbf{k}} = \Sigma_a(\mathbf{k}, \varepsilon = 0)$ is calculated by the analytic continuation $i\varepsilon_n \rightarrow \varepsilon + i\delta$ from the anomalous self-energy term $\Sigma_a(k)$. It is important that Yosida function is expressed as a universal even function of $y = \Delta_{\mathbf{k}}^*/T$:

$$g(y) = \int_{-\infty}^{\infty} e^{\sqrt{x^2+y^2}} \left(1 + e^{\sqrt{x^2+y^2}} \right)^{-2} dx. \quad (39)$$

The graph of $1-g(y)$ for $y > 0$ is shown in Fig.2. Note that $1-g(0) = 0$ and $1-g(\pm\infty) = 1$, respectively. This indicates that $1-Y(\mathbf{k}; T) = 0$ at $T = T_c$, since $\Delta_{\mathbf{k}}^* = 0$, while $1-Y(\mathbf{k}; T) = 1$ at $T = 0$, and that the increase in $y = \Delta_{\mathbf{k}}^*/T$ results in the increase in λ^{-2} via Yosida function. According to Ref.1, $\bar{v}_{\nu}^*(\mathbf{k}') = v_{\nu}^*(\mathbf{k}')$ at $T = T_c$ and $\bar{v}_{\nu}^*(\mathbf{k}') = \bar{j}_{\nu}^*(\mathbf{k}')$ at $T = 0$. This means that $\bar{v}_{\nu}^*(\mathbf{k}')$ is suppressed near $T = 0$ compared to that near $T = T_c$. From these facts, the

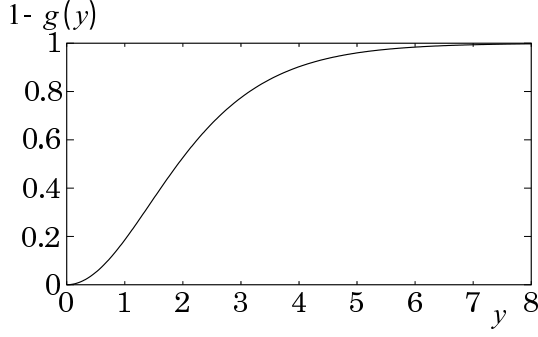


Fig. 2. The graph of $1 - g(y)$. For $y > 0$, $1 - g(y)$ increases monotonically from zero at $y = 0$ to unity at $y = \infty$.

inverse square of the penetration depth at $T = 0$ is given by

$$\lambda_{\mu\nu}^{-2}|_{T=0} = 8\pi \int_{FS} \frac{dS_{\mathbf{k}'}}{(2\pi)^3 |v_{\mathbf{k}'}^*|} v_{\mathbf{k}'\mu}^* \bar{j}_{\mathbf{k}'\nu}^*. \quad (40)$$

Here, $\bar{j}_{\mathbf{k}}^*$ is the current carried by quasiparticles in the superconducting state and $v_{\mathbf{k}}^*$ is the renormalized velocity of quasiparticles in the normal state, respectively. According to Refs.1 and 2, $\bar{j}_{\mathbf{k}}^*$ coincides with $j_{\mathbf{k}}^*$ due to the cancellation of the change of the velocity $\bar{v}_{\mathbf{k}}^* - v_{\mathbf{k}}^*$ and the change of the backflow effect. Therefore we use $j_{\mathbf{k}}^*$ instead of $\bar{j}_{\mathbf{k}}^*$ hereafter. The velocity of quasiparticle $v_{\mathbf{k}}^*$ is expressed as

$$v_{\mathbf{k}}^* = z_{\mathbf{k}} \frac{\partial}{\partial \mathbf{k}} (\varepsilon_{\mathbf{k}} + \text{Re} \Sigma_n^R(\mathbf{k}, \varepsilon = 0)) \equiv \frac{\partial \varepsilon_{\mathbf{k}}^*}{\partial \mathbf{k}}. \quad (41)$$

After rather long calculation,² $j_{\mathbf{k}}^*$ is expressed as

$$j_{\mathbf{k}}^* = v_{\mathbf{k}}^* + z_{\mathbf{k}} w_{\mathbf{k}}^R(0), \quad (42)$$

where

$$w_{\mathbf{k}}^R(0) = u_{\mathbf{k}}^R(0) + \frac{1}{N} \sum_{\mathbf{k}'} \int \frac{d\varepsilon'}{2\pi} \left[\coth \frac{\varepsilon'}{2T} \text{Im} V_{\mathbf{k}-\mathbf{k}'}^R(-\varepsilon') \frac{\partial \text{Re} G_{\mathbf{k}'}^R(\varepsilon')}{\partial \varepsilon'} + \tanh \frac{\varepsilon'}{2T} \frac{\partial \text{Re} V_{\mathbf{k}-\mathbf{k}'}^R(-\varepsilon')}{\partial \varepsilon'} \text{Im} G_{\mathbf{k}'}^R(\varepsilon') \right] z_{\mathbf{k}'} w_{\mathbf{k}'}^R(0), \quad (43)$$

$$u_{\mathbf{k}}^R(0) = \frac{1}{N} \sum_{\mathbf{k}'} \int \frac{d\varepsilon'}{2\pi} \left[\coth \frac{\varepsilon'}{2T} \text{Im} V_{\mathbf{k}-\mathbf{k}'}^R(-\varepsilon') \frac{\partial \text{Re} G_{\mathbf{k}'}^R(\varepsilon')}{\partial \varepsilon'} + \tanh \frac{\varepsilon'}{2T} \frac{\partial \text{Re} V_{\mathbf{k}-\mathbf{k}'}^R(-\varepsilon')}{\partial \varepsilon'} \text{Im} G_{\mathbf{k}'}^R(\varepsilon') \right] (v_{\mathbf{k}'} - v_{\mathbf{k}}). \quad (44)$$

$z_{\mathbf{k}} = \left(1 - \frac{\partial \text{Re} \Sigma_n^R(\mathbf{k}, \varepsilon)}{\partial \varepsilon} \Big|_{\varepsilon=0} \right)^{-1}$ is the renormalization factor. $\Sigma_n^R(\mathbf{k}, \varepsilon)$ and the retarded Green's function $G_{\mathbf{k}}^R(\varepsilon)$ is calculated by the analytic continuation $i\varepsilon_n \rightarrow \varepsilon + i\delta$ from $\Sigma_n(k)$ and $G(k)$, respectively. Similarly, $V_{\mathbf{k}}^R(\varepsilon)$ is derived by the analytic continuation $i\omega_n \rightarrow \varepsilon + i\delta$ from the normal vertex $V(k)$.

Note that $j_{\mathbf{k}}^* = \bar{v}^*(\mathbf{k})|_{T=0}$ is lowered compared to $v_{\mathbf{k}}^* = \bar{v}^*(\mathbf{k})|_{T=T_c}$. This difference is called the vertex correction, which is considered as the backflow effect. According to Ref.22, the vertex correction is more effective, when the antiferromagnetic spin fluctuation is strong, such as in the underdoped LSCO. The penetration depth $\lambda_{0\mu\nu}^{-2}$ without including the vertex correction is expressed by

$$\lambda_{0\mu\nu}^{-2} = 8\pi \int_{FS} \frac{dS_{\mathbf{k}'}}{(2\pi)^3 |v_{\mathbf{k}'}^*|} v_{\mathbf{k}'\mu}^* (1 - Y(\mathbf{k}'; T)) v_{\mathbf{k}'\nu}^*, \quad (45)$$

$$\lambda_{0\mu\nu}^{-2}|_{T=0} = 8\pi \int_{FS} \frac{dS_{\mathbf{k}'}}{(2\pi)^3 |v_{\mathbf{k}'}^*|} v_{\mathbf{k}'\mu}^* v_{\mathbf{k}'\nu}^*. \quad (46)$$

Owing to the vertex correction, $\lambda_{\mu\nu}^{-2}|_{T=0}$ is lowered compared to $\lambda_{0\mu\nu}^{-2}|_{T=0}$. Since the vertex correction is effective only near $T = 0$, $\lambda_{\mu\nu}^{-2}$ is suppressed near $T = 0$ under the strong antiferromagnetic fluctuation. In order to calculate $\lambda_{0\mu\nu}^{-2}$ at finite temperature $0 < T < T_c$, we have to calculate it in the superconducting state, since Eq.45 contains Yosida function. We calculate $\lambda_{0\mu\nu}^{-2}$ using Eqs.45, 38 and 41, in which Green's functions and self-energy terms are calculated by Eqs.11-17. Although the vertex correction is not included in $\lambda_{0\mu\nu}^{-2}$, it expresses the behavior of $\lambda_{\mu\nu}^{-2}$ near $T = T_c$ correctly where the vertex correction is not effective. This fact means that we can discuss the development of $\lambda_{\mu\nu}^{-2}$ just below T_c using the result of $\lambda_{0\mu\nu}^{-2}$.

6. The Pressure Dependence of the Parameters

In this section, we discuss how the parameters in our model depend on the pressure. We assume that the dependence of the Coulomb repulsion U on the pressure is weaker than those of the hopping terms t and t' . On the other hand, the absolute values of t and t' increase under high pressure, since the lattice constant of κ -(ET)₂Cu(NCS)₂ decreases due to compression. Owing to the large isothermal compressibility,²³ κ -(ET)₂Cu(NCS)₂ is quite sensitive to the pressure. Since the bandwidth W is approximately proportional to t , the large value of t results in small ratio of U/W which indicates the weak electron correlation.

Moreover, we need to take account of the change of t'/t under pressure. In Refs.5 and 6, t'/t and the effective mass ratio for α -pocket electron m_{α}^*/m_e under pressure are measured by Shubnikov-de-Haas effect in both κ -(*d*₈ET)₂Cu(NCS)₂ and κ -(*h*₈ET)₂Cu(NCS)₂. According to these results, the decrease in T_c , that in m_{α}^*/m_e , and the increase in t'/t are observed as the hydrostatic pressure increases. The decrease in T_c is similar to the case of other organic superconductors.²⁴ The decrease in the effective mass ratio is observed also by the infrared reflectivity experiment.²⁵ The stronger pressure dependence of t'/t , T_c and m_{α}^*/m_e in κ -(*d*₈ET)₂Cu(NCS)₂⁵ compared to that in κ -(*h*₈ET)₂Cu(NCS)₂⁶ is considered to result from the different pressure medium used in the two experiments. In fact, the isotope effect for T_c is small, when the same pressure medium is used.⁷ We can consider that T_c under pressure depends strongly on the pressure medium.

In κ -(*d*₈ET)₂Cu(NCS)₂, the ratio t'/t varies from about 0.7 at $P = 0$ to about 0.77 at

$P = 0.1\text{GPa}$. The fact that t'/t increases under pressure indicates that t' is more sensitive to the pressure than t . On the other hand, m_α^*/m_e varies from 3.5 at $P = 0$ to 2.5 at $P = 0.1\text{GPa}$. The change of t'/t results in the change of the Fermi surface. When t'/t is large, the lattice structure is near to the triangular lattice, and the Fermi surface is far from the antiferromagnetic Brillouin zone boundary as shown in Fig.8. Therefore the antiferromagnetic fluctuation becomes weaker as t'/t increases with the fixed value of U . From these reasons, we can say that the electron correlation and the antiferromagnetic fluctuation in $\kappa\text{-(ET)}_2\text{Cu(NCS)}_2$ are strong under low pressure compared with those under high pressure. In our model, we assume that the value of U is independent of the pressure and that the values of t/U and t'/t vary with the pressure. From now on, we take U as the unit of energy, since it is assumed to be unchanged. In our model, W and the strength of electron correlation mainly depend on t/U . On the other hand, the shape of the Fermi surface is changed by t'/t . Note that the antiferromagnetic fluctuation becomes weaker as t'/t increases with the constant value of U .

7. Result and Discussion

In our numerical calculation, we divide the first Brillouin zone into 128×128 meshes in the \mathbf{k} -space and take 4096 Matsubara frequencies. In this condition, the obtained results are reliable with temperature T down to approximately $0.001t$. Within the FLEX approximation, we calculate $v_{\mathbf{k}x}^*$, $j_{\mathbf{k}x}^*$, $\lambda_0^{-2}|_{T=0}$ and $\lambda^{-2}|_{T=0}$ by using Eqs.41, 42-44, 46 and 40 respectively. The results are shown in Figs. 3-7. From now on, we calculate only λ_{xx}^{-2} and refer to it as the in-plane penetration depth $\lambda_{\mu\nu}^{-2}$, since the qualitative behavior of $\lambda_{\mu\nu}^{-2}$ is similar in all directions within the xy -plane. We abbreviate the subscripts xx and denote λ_{xx}^{-2} as λ^{-2} hereafter. In the calculations of $\lambda_0^{-2}|_{T=0}$ and $\lambda^{-2}|_{T=0}$, the temperature at which the calculation is performed is important. In order to calculate Eqs.40 and 46 precisely, we need to obtain the values of $v_{\mathbf{k}x}^*$ and $j_{\mathbf{k}x}^*$ at $T = 0$ by extrapolation of $v_{\mathbf{k}x}^*$ and $j_{\mathbf{k}x}^*$ obtained at finite temperatures. However, the extrapolation of $j_{\mathbf{k}x}^*$ is difficult, since the numerical error in the calculation increases in the low temperature region. Therefore $v_{\mathbf{k}x}^*$, $j_{\mathbf{k}x}^*$, $\lambda_0^{-2}|_{T=0}$ and $\lambda^{-2}|_{T=0}$ shown in Figs.3-5 and 7 are calculated with the temperature fixed to $T = 0.0014U$. Although the calculations are not correct, it is enough to investigate the qualitative behavior of the vertex correction.

Figure 3 shows that $j_{\mathbf{k}x}^*$ is lowered compared to $v_{\mathbf{k}x}^*$ by the vertex correction within the FLEX approximation. Note that the ratio of the vertex correction $(j_{\mathbf{k}x}^* - v_{\mathbf{k}x}^*)/v_{\mathbf{k}x}^*$ is approximately constant everywhere on the Fermi surface in Fig.3. This is in contrast to that in underdoped cuprates calculated in Ref.1. In the cuprates, $(j_{\mathbf{k}x}^* - v_{\mathbf{k}x}^*)^*/v_{\mathbf{k}x}^*$ is large at hot spots compared to that at cold spots. This implies that in $\kappa\text{-(ET)}_2\text{Cu(NCS)}_2$ the difference between hot spots and cold spots (see Fig.8) on the Fermi surfaces is small in contrast to the underdoped cuprates, as long as the temperature near $T = 0$ is concerned. Figure 4 shows $\bar{z}_{\mathbf{k}}^{-1}$, $\lambda_0^{-2}|_{T=0}$, and $\lambda^{-2}|_{T=0}$ for various values of t/U with $t'/t = 0.7$, where $z^{-1} = \bar{z}_{\mathbf{k}}^{-1}$ is the average of $z_{\mathbf{k}}^{-1}$ over the Fermi surface. The factor z^{-1} is considered to be approximately pro-

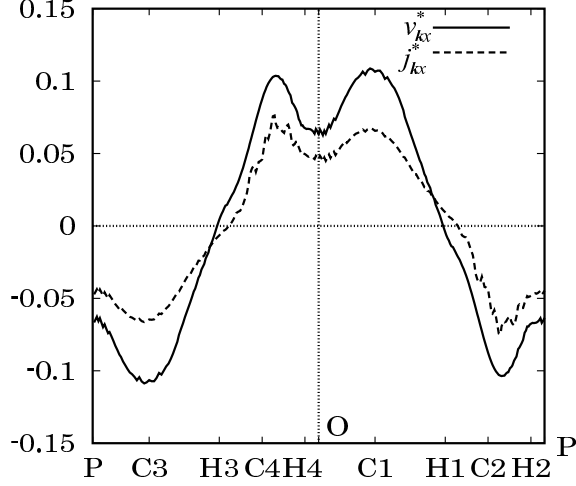


Fig. 3. The current and the renormalized velocity on the FS for $t/U = 0.20$, $t'/t = 0.7$ and the temperature $T = 0.0014U$ within FLEX. The points O,P,C1-C4,H1-H4 correspond to those in Fig.8.

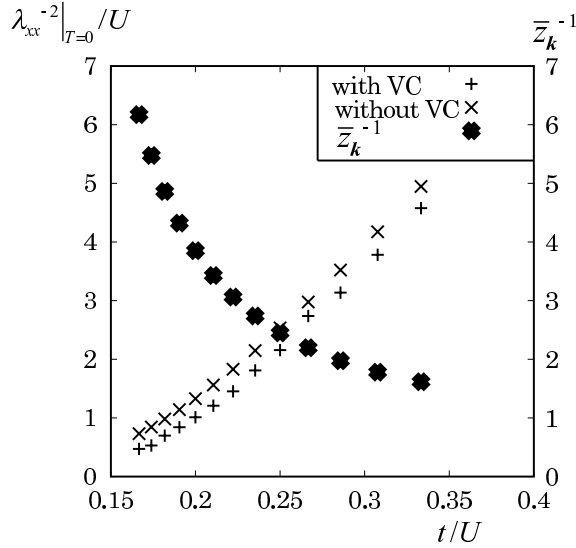


Fig. 4. $\lambda_{xx}^{-2}|_{T=0}$ (with VC), $\lambda_{xx}^{-2}|_{T=0}$ (without VC) and \bar{z}_k^{-1} calculated by FLEX. Low value of t/U corresponds to the strong electron correlation and high value to the weak one. the ratio t'/t is fixed to 0.7. The vertex correction reduces largely the value of λ_{xx}^{-2} compared to λ_{xx}^{-2} , when the electron correlation is strong.

portional to m_a^*/m_e . Figure 5 shows that the effect of the vertex correction within SC-SOPT is quite small compared to that in the FLEX shown in Fig. 4. This is similar to the results in Ref.2. Figure 6 shows the dependence of T_c on t/U with $t'/t = 0.7$ calculated within FLEX and within TOPT. The value of T_c increases as t/U decreases both for FLEX and for TOPT. For TOPT, small value of t/U is required for superconductivity and T_c decreases rapidly as t/U increases compared to T_c calculated within FLEX. These results are consistent with the

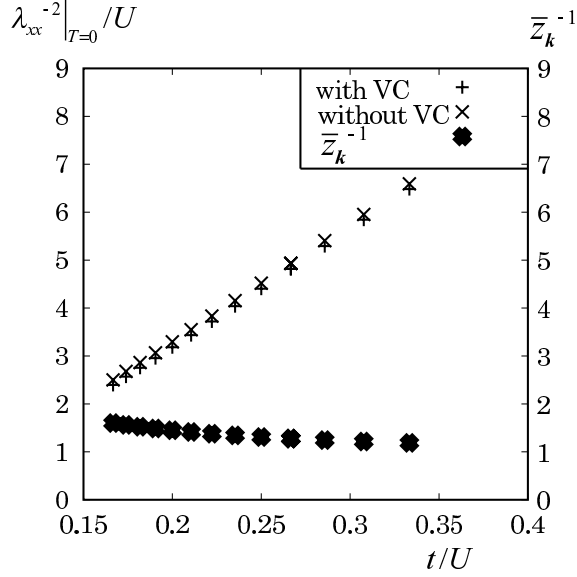


Fig. 5. $\lambda^{-2}|_{T=0}$ (with VC), $\lambda_0^{-2}|_{T=0}$ (without VC) and \bar{z}_k^{-1} calculated by SC-SOPT. t'/t is fixed to 0.7. The reduction of λ^{-2} by the effect of the vertex correction is quite small compared to Fig.4.

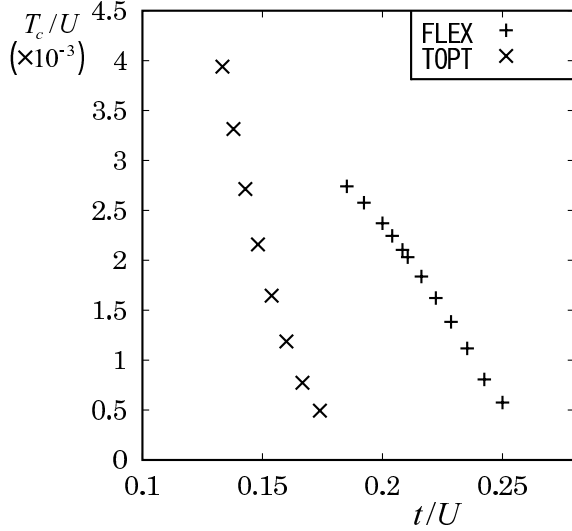


Fig. 6. The dependence of T_c on t/U with $t'/t = 0.7$ within FLEX and TOPT. Both for FLEX and for TOPT, T_c is higher when the electron correlation is strong, that is, t/U is small. T_c decreases more rapidly as t/U increases for TOPT than for FLEX.

calculations in Refs.13, 14 and 15. From Fig.4, we can see that $(\lambda_0^{-2}|_{T=0} - \lambda^{-2}|_{T=0}) / \lambda_0^{-2}|_{T=0}$ increases as t/U decreases. This means that the suppression of $\lambda^{-2}|_{T=0}$ by the vertex correction is large under the strong electron correlation, even if the shape of the Fermi surface is unchanged. Moreover, $\lambda_0^{-2}|_{T=0}$ itself decreases as t/U decreases. This is because $\lambda_0^{-2}|_{T=0}$ is approximately proportional to zt , or zW , where $z = (m^*/m)^{-1}$ is the average of the renormalization factor on the Fermi surface. Shortly to say, the strong electron correlation

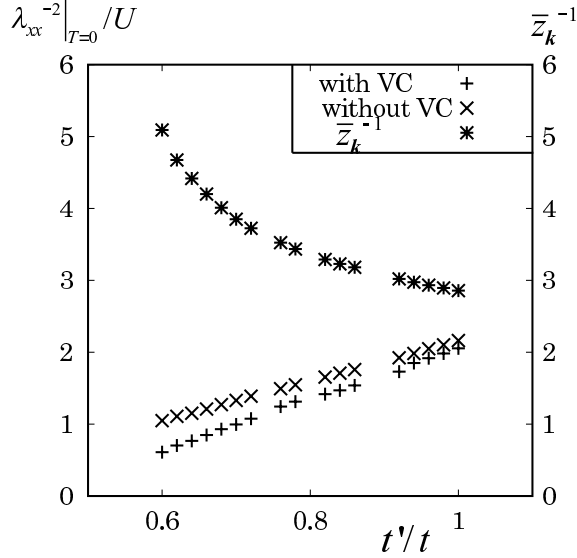


Fig. 7. The t'/t dependence of z_k^{-1} , $\lambda_0^{-2}|_{T=0}$ and $\lambda_{xx}^{-2}|_{T=0}$ with $t/U = 0.200$ within FLEX. The small value of t'/t corresponds to the strong antiferromagnetic spin fluctuation, while the large value to the weak fluctuation. The vertex correction affects strongly under the strong antiferromagnetic fluctuation.

suppresses $\lambda^{-2}|_{T=0}$ through the increase of the vertex correction effect and the strong mass renormalization which corresponds to the decrease in z .

Figure 7 shows the t'/t dependence of z^{-1} , $\lambda_0^{-2}|_{T=0}$ and $\lambda^{-2}|_{T=0}$ with $t/U = 0.200$, calculated within FLEX. On the other hand, Fig.9 shows the t'/t dependence of T_c within FLEX and within TOPT. Both in FLEX and in TOPT, T_c increases as t'/t decreases and the dependence is quite similar to each other. According to Fig.7, $(\lambda_0^{-2}|_{T=0} - \lambda^{-2}|_{T=0})/\lambda_0^{-2}|_{T=0}$ increases as t'/t decreases. This means that the effect of the vertex correction in $\lambda^{-2}|_{T=0}$ is strong under the strong antiferromagnetic fluctuation. Moreover, $\lambda^{-2}|_{T=0}$ decreases approximately in proportion to z as t'/t decreases. Then with similar discussion to the dependence on t/U , $\lambda^{-2}|_{T=0}$ is suppressed by the effect of vertex correction and by the decrease in z , when t'/t is small.

Under low pressure, the strong electron correlation and the strong antiferromagnetic fluctuation exist. In our model, the decrease in t/U and that in t'/t under low pressure indicate the strong electron correlation and the strong antiferromagnetic fluctuation, respectively. These effects result in the strong mass renormalization and the increase in the vertex correction effect. The suppression of $\lambda^{-2}|_{T=0}$ under low pressure results from these effects. On the other hand, the increase of T_c under low pressure is also explained by the strong electron correlation and the antiferromagnetic fluctuation.

Let us consider the justification of our calculation by estimating the parameters. By comparing our result for z^{-1} in Figs.3-7 with the value of m_{α}^*/m_e and t'/t measured in Ref.5, we

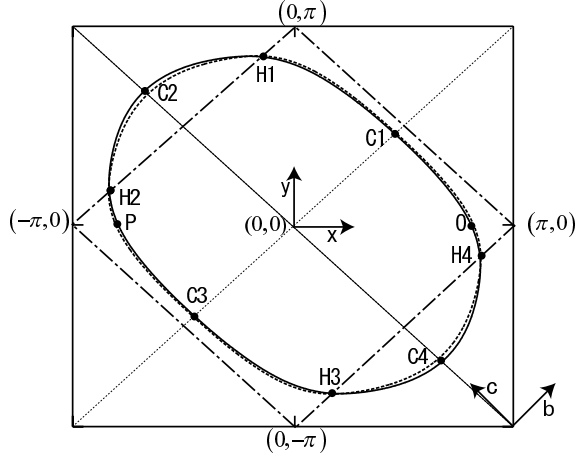


Fig. 8. The Fermi surfaces of κ -(ET) $_2$ Cu(NCS) $_2$ with $t'/t = 0.7$ (dotted line) and 0.75 (solid line), where t/U is fixed to 0.200 . The shape of the Fermi surfaces is consistent with the estimation from the Shubnikov-de-Haas effect. The crossing points of the FS and the antiferromagnetic Brillouin zone boundary shown by the dash dotted line are the hot spots, which are denoted by H1-H4. On the other hand, the crossing points of the FS and the gap nodes shown by two diagonal lines are the cold spots, which are denoted by C1-C4. Note that the axes are rotated by $\pi/4$ compared to the FS in Refs.5 and 26.

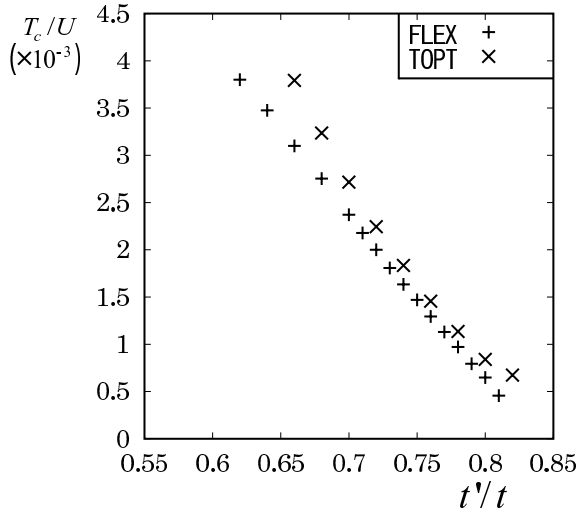


Fig. 9. The dependence of T_c on t'/t within FLEX and TOPT. The former is calculated with $t/U = 0.200$, and the latter with $t/U = 0.154$. Both for FLEX and TOPT, T_c is higher under strong antiferromagnetic fluctuations, or small value of t'/t .

can estimate the parameters in the calculation for κ -(d_8 ET) $_2$ Cu(NCS) $_2$. For convenience, we assume z^{-1} to be equivalent to m_α^*/m_e in the estimation. Judging from the values of z^{-1} , the FLEX approximation is more appropriate for κ -(d_8 ET) $_2$ Cu(NCS) $_2$ than SC-SOPT. From this reason, we take account of only the FLEX approximation in the discussion of λ^{-2} hereafter.

Then, we estimate $t/U = 0.208$ at $P = 0$ from $z^{-1} = 3.5$ and $t'/t = 0.7^5$ and $t/U = 0.237$ at $P = 0.1\text{GPa}$ from $z^{-1} = 2.5$ and $t'/t = 0.77$, by using the result within FLEX. From the above estimation, we can compare the calculated T_c with the measured one. Since the value of t at $P = 0$ is estimated⁶ as $0.12\text{eV} \sim 1400\text{K}$ from the polarized infrared reflectance measurements,²⁷ U is estimated as approximately 6700K . Using these parameters, we calculate $T_c = 2.08 \times 10^{-3}U = 14\text{K}$ at $P = 0$, and $T_c = 2.3 \times 10^{-4}U = 1.5\text{K}$ at $P = 0.1\text{GPa}$ within FLEX. The value of T_c measured by experiment for $\kappa\text{-(d}_8\text{ET)}_2\text{Cu(NCS)}_2$ is approximately 10K at $P = 0$ and 6K at $P = 0.1\text{GPa}$,^{7,28} although it depends strongly on the pressure medium. Considering that the calculated T_c has delicate dependence on the parameters, we can say that the calculated T_c is in magnitude consistent with the measured T_c and that our model and calculation are justified.

Next, we discuss the development of λ^{-2} just below T_c in $\kappa\text{-(d}_8\text{ET)}_2\text{Cu(NCS)}_2$. We calculate λ_0^{-2} for $0 < T < T_c$ according to Eq.45. As a matter of fact, λ_0^{-2} develops rapidly just below T_c , when t/U and t'/t are small, as shown in Figs.10 and 11. Figure 10 shows the λ_0^{-2} - T diagram with $t/U = 0.222$, $t'/t = 0.7$ and with $t/U = 0.200$, $t'/t = 0.7$. On the other hand, Fig.11 shows the diagram with $t/U = 0.200$, $t'/t = 0.7$ and with $t/U = 0.200$, $t'/t = 0.75$. Although the effect of vertex correction is not included in λ_0^{-2} , these diagrams express qualitatively correct development of λ^{-2} just below T_c , since $\lambda_0^{-2} = \lambda^{-2}$ at $T = T_c$.^{1,2} From Figs.10 and 11, we can see that λ_0^{-2} has a linear dependence on T near $T = 0$:

$$\lambda_0^{-2} - \lambda_{0*}^{-2}|_{T=0} \propto T, \quad (47)$$

where $\lambda_{0*}^{-2}|_{T=0}$ is obtained from extrapolation of λ_0^{-2} calculated by Eq.45 to $T = 0$. The linear dependence of λ_0^{-2} results from the existence of the line-node in the superconducting gap. $\lambda_{0*}^{-2}|_{T=0}$ does not coincide with $\lambda_0^{-2}|_{T=0}$ shown in Figs.4 and 7. This is because the results in Figs.4 and 7 are calculated with $T = 0.0014U$ and are not extrapolated to $T = 0$, owing to the difficulties in calculating $j_{\mathbf{k}x}^*$ just near $T = 0$. Since $v_{\mathbf{k}x}^*$ can be calculated just near $T = 0$, we can extrapolate Eq.46 to $T = 0$. The difference between $\lambda_{0*}^{-2}|_{T=0}$ and the result of extrapolation of Eq.46 is less than 3%. This indicates that the calculation of Eq.45 and that of Eq.46 are consistent with each other.

For the convenience in comparison, we normalize these diagrams by T_c and $\lambda_{0*}^{-2}|_{T=0}$. The results of the normalization for Figs.10 and 11 are shown by Figs.12 and 13, respectively. In Figs.12 and 13, the development of λ_0^{-2} just below T_c with $t/U = 0.200$ and $t'/t = 0.7$ is more rapid than that with $t/U = 0.222$ and $t'/t = 0.7$, or than that with $t/U = 0.200$ and $t'/t = 0.75$. This indicates that the strong electron correlation and the strong antiferromagnetic fluctuation are the main origin of the rapid development of λ^{-2} just below T_c under low pressure in Ref.3.

The rapid development of λ_0^{-2} just below T_c implies that $\Delta_{\mathbf{k}}^*/T$ develops rapidly. The temperature dependence of $\Delta_{\mathbf{k}_{\text{max}}}^*/T$ is shown in Fig.14, where $\Delta_{\mathbf{k}_{\text{max}}}^*$ is the maximum of $\Delta_{\mathbf{k}}^*$

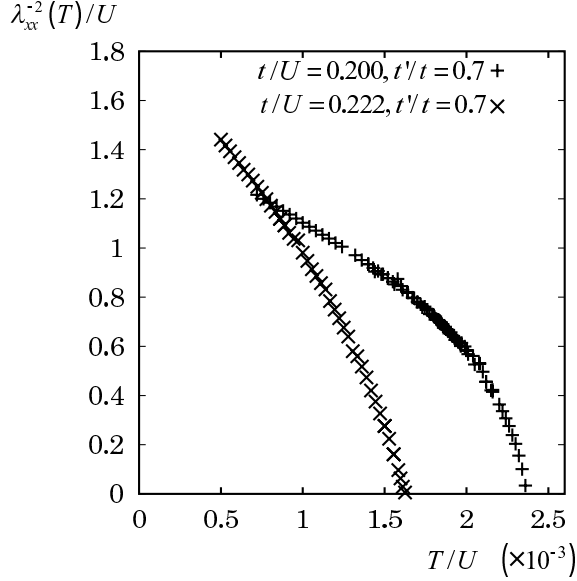


Fig. 10. λ_0^{-2} - T diagram for $(t/U = 0.222, t'/t = 0.7)$ and for $(t/U = 0.200, t'/t = 0.7)$. $T_c = 1.63 \times 10^3 U$ in the former, and $2.37 \times 10^3 U$ in the latter.

on the Fermi surface. In Fig.14, $\Delta_{\mathbf{k}_{\max}}^*/T$ develops rapidly with $t/U = 0.200$ and $t'/t = 0.700$, compared to that with $t/U = 0.222$ and $t'/t = 0.700$, or to that with $t/U = 0.200$ and $t'/t = 0.750$. This indicates that the strong antiferromagnetic fluctuation and the strong electron correlation cause the rapid development of $\Delta_{\mathbf{k}_{\max}}^*/T$, which result in the rapid development of λ_0^{-2} . Figures 12, 13, and 14 justify the conclusion that the increases in $\Delta_{\mathbf{k}}^*/T$ is the dominant cause of the development of λ_0^{-2} . The pseudogap effect is also considered to be the cause of the rapid development of $\Delta_{\mathbf{k}}^*$ just below T_c , although it can not be calculated in the framework of this paper. The pseudogap arises from the superconducting fluctuation as discussed by Jujo, *et al.*²⁹ In fact, the pseudogap effect in κ -(d_8 ET) $_2$ Cu(NCS) $_2$ is observed up to $T = 45$ K in STM spectroscopy at ambient pressure.^{30,31} Although similar measurements under pressure are not performed, it is natural to consider that the pseudogap effect is weak or disappears under pressure owing to the weak electron correlation and the weak antiferromagnetic fluctuation. If the pseudogap exists above T_c , then the superconducting gap $\Delta_{\mathbf{k}}^*$ develops rapidly when the superconducting state is realized at $T = T_c$ as shown in Ref.32.

Last, we discuss the uniaxial pressure dependence of T_c . We are not able to calculate the effect of the interlayer pressure applied parallel to a -axis, since we adopt Q2D band structure and ignore the interlayer hopping term. Nevertheless, we can presume that the three-dimensionality is strong under the interlayer pressure and it is generally understood that T_c is suppressed under strong three-dimensionality as calculated in Refs.33 and 34. For the b -axis pressure, the behavior of T_c is easily explained. Under the b -axis pressure, both t and t' increase. Since the increase in t is small and that in t' is large under the b -axis pressure

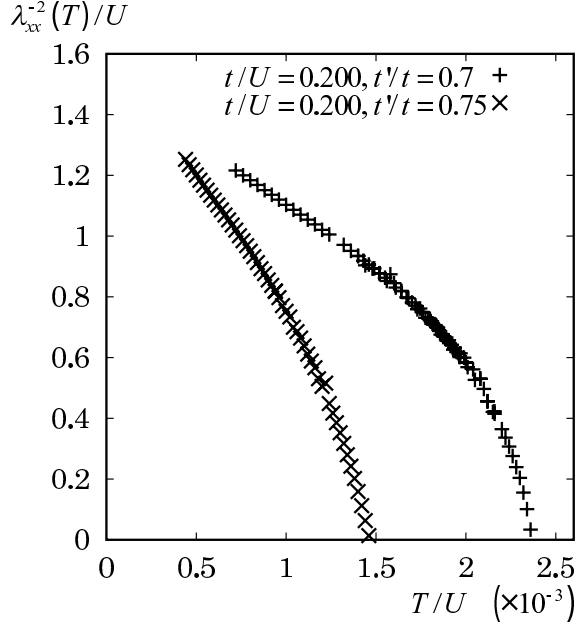


Fig. 11. λ_0^{-2} - T diagram for $(t/U = 0.200, t'/t = 0.7)$ and for $(t/U = 0.200, t'/t = 0.75)$. $T_c = 2.37 \times 10^3 U$ in the former, and $1.47 \times 10^3 U$ in the latter.

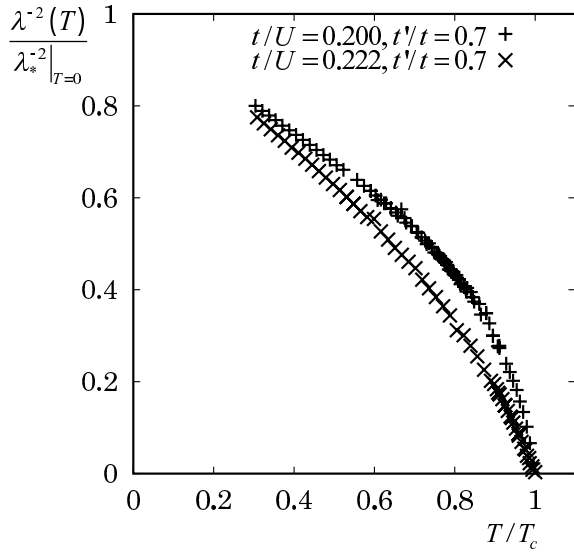


Fig. 12. λ_0^{-2} - T diagram for $(t/U = 0.222, t'/t = 0.7)$ and for $(t/U = 0.200, t'/t = 0.7)$. This diagram is normalized by $T = T_c$ and $\lambda_0^{-2} = \lambda_0^{-2}|_{T=0}$, respectively. λ_0^{-2} shows rapid development under the strong electron correlation. ($t/U = 0.200$)

compared to those under the hydrostatic pressure, it is sure that both t'/t and t/U increase under the b -axis pressure. Therefore we can say that the b -axis pressure suppresses T_c similarly to the hydrostatic pressure from the discussion above.

Then we discuss the behavior of T_c under the c -axis pressure. Since the c -axis is perpendic-

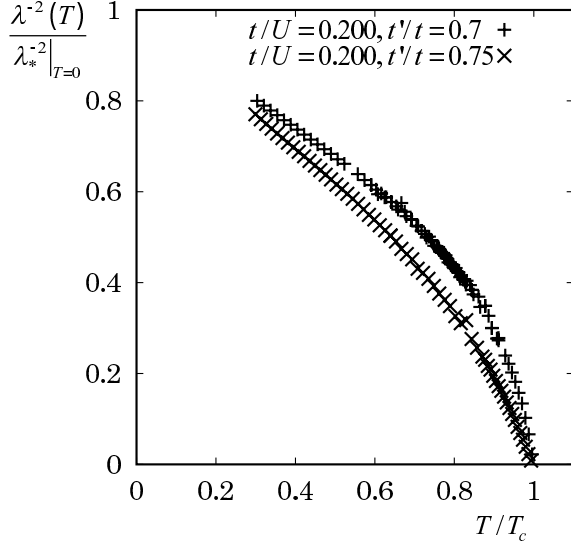


Fig. 13. λ_0^{-2} - T diagram for $(t/U = 0.200, t'/t = 0.7)$ and for $(t/U = 0.200, t'/t = 0.75)$. This diagram is normalized by $T = T_c$ and $\lambda_0^{-2} = \lambda_0^{-2}|_{T=0}$, respectively. λ_0^{-2} shows rapid development under the strong antiferromagnetic fluctuation. ($t'/t = 0.70$)

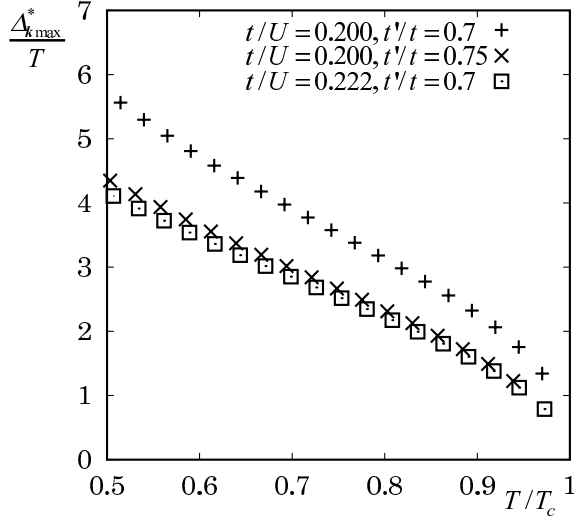


Fig. 14. The temperature dependence of $\Delta_{k_{\max}}^*/T$ with $t/U = 0.200$ and $t'/t = 0.700$, with $t/U = 0.222$ and $t'/t = 0.700$, and with $t/U = 0.200$ and $t'/t = 0.750$. $\Delta_{k_{\max}}^*/T$ with $t/U = 0.200$ and $t'/t = 0.700$ develops most rapidly.

ular to the direction of the hopping term t' , it is natural to assume that t' is constant and that t increases under the c -axis pressure. Moreover, U is assumed to be constant with increasing c -axis pressure. These assumptions indicate that t/U increases and t'/t decreases. The former corresponds to the suppression of the electron correlations and the latter to the deformation of the Fermi surface, which approaches the antiferromagnetic Brillouin zone boundary. These two effects are competitive to each other for T_c : the former decreases T_c and the latter increases

it.

Figures 15 and 16 show the behavior of T_c under the c -axis pressure calculated within FLEX and TOPT, respectively. For FLEX, T_c tends to increase rapidly up to $t/U = 0.28$ and the decrease over $t/U = 0.28$ is rather slow. The value of $t/U = 0.28$ corresponds to rather higher pressure than 1kbar, considering that the increase of t under the uniaxial pressure is smaller than that under the hydrostatic pressure. As a conclusion, the value of T_c within FLEX increases as the c -axis pressure increases, since the deformation of the Fermi surface affects strongly compared to the suppression of the electron correlation. This behavior of T_c is consistent with the results in Refs.8 and 9 below 1kbar. This fact implies that the antiferromagnetic fluctuation is strong under the weak c -axis pressure. On the other hand, T_c calculated by TOPT increases slightly up to $t/U = 0.16$ and then decreases rather rapidly. The difference between FLEX and TOPT is mainly due to the t/U dependences of T_c shown in Fig.6. T_c by TOPT depends rather strongly on t/U than that by FLEX, while the t'/t dependences differ little. Although it is quite difficult to estimate the value of t/U for TOPT, we estimate t/U at ambient pressure to be from 0.15 to 0.16 judging from the value of $T_c \sim 11\text{K}$ and $t \sim 1400\text{K}$. Therefore, T_c calculated within TOPT decreases under the c -axis pressure, since the suppression of the electron correlation is dominant over the deformation of the Fermi surface. This behavior of T_c is consistent with the experimental results^{8,9} on T_c under the c -axis pressure above 1kbar. It implies that the antiferromagnetic fluctuation is weak under the high c -axis pressure. As a conclusion, we can explain the behavior of T_c under the c -axis pressure by considering two competitive effects: the suppression of the electron correlation and the approach of the Fermi surface to the antiferromagnetic Brillouin zone boundary. In the low c -axis pressure region, the latter effect is dominant and FLEX approximation is valid. On the other hand, in the high pressure region the former effect is dominant and TOPT is valid.

8. Conclusion

Under low pressure, the development of λ^{-2} just below T_c in $\kappa\text{-(ET)}_2\text{Cu(NCS)}_2$ is rapid and λ^{-2} near $T = 0$ is suppressed, when they are compared to those under high pressure. These effects, added to the increase of T_c , result from the strong electron correlation and the strong antiferromagnetic fluctuation under low pressure. This is due to the decrease in t/U and that in t'/t . In cuprates, the Fermi surface changes with the change of doping, and the antiferromagnetic spin fluctuation is enhanced in underdoped cuprates, while the renormalization factor z and the bandwidth depend weakly on the doping.^{1,2} Then the suppression of λ^{-2} near $T = 0$ in underdoped cuprates are mainly due to the vertex correction. On the other hand, the explanation of the pressure dependence of λ^{-2} in $\kappa\text{-(ET)}_2\text{Cu(NCS)}_2$ is rather complicated. Under low pressure, the narrow bandwidth W and the strong antiferromagnetic fluctuation are observed. The former effect results in the strong electron correlation and the

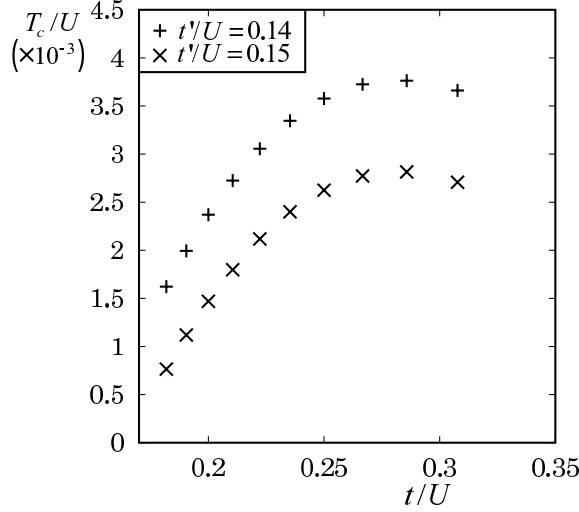


Fig. 15. The c -axis pressure dependence of T_c calculated within FLEX. The value of t'/U is fixed to 0.14 (which has higher T_c) and 0.15(lower). T_c tends to increase rapidly up to t/U becomes 0.28.

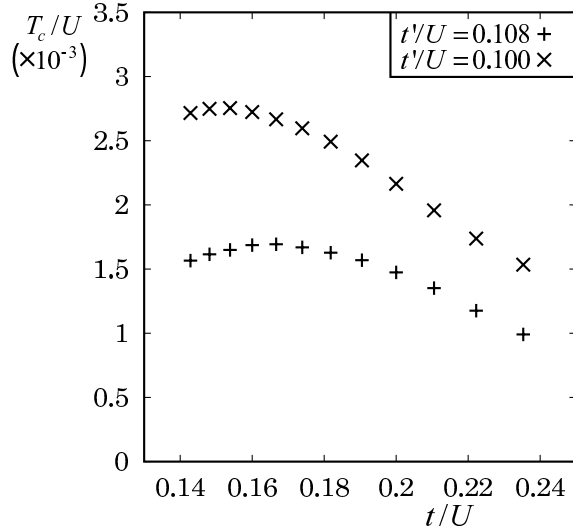


Fig. 16. The c -axis pressure dependence of T_c calculated within TOPT. The value of t'/U is fixed to 0.100 (which has higher T_c) and 0.108(lower). T_c slightly increases up to $t/U = 0.16$ and then decreases rapidly.

decrease in z , while the latter enhances the vertex correction. In short, the decrease in z and the effect of the vertex correction are all the origins of the suppression of λ^{-2} at $T = 0$.

The rapid development of λ^{-2} just below T_c under low pressure in κ -(ET)₂Cu(NCS)₂ is explained by the rapid development of the superconducting gap. The superconducting gap develops rapidly just below T_c under low pressure, since the strong antiferromagnetic fluctuation and the strong electron correlation exist. Moreover, the pseudogap effect is also considered to cause the rapid development of the superconducting gap, although it is not

studied in this paper. This is similar to the case of cuprates. In cuprates, the strong pseudogap effect is observed in the underdoped region where the antiferromagnetic fluctuation is strong, and λ^{-2} develops rapidly just below T_c compared to that in the overdoped region.

As a conclusion, we have explained various experimental results on κ -(ET)₂Cu(NCS)₂ under pressure, *e.g.* λ^{-2} near $T = 0$, the development of λ^{-2} just below T_c , the superconducting transition temperature under the hydrostatic pressure and that under the uniaxial pressure. In the explanation, we adopted Hubbard model and assumed that the electron correlation and the antiferromagnetic fluctuation are suppressed under pressure. Then the obtained results are consistent with the measurements, which indicates that our assumption is appropriate.

The numerical calculation was performed by sx5 in Yukawa Institute Computer Facility, Kyoto University.

References

- 1) T. Jujo: J. Phys. Soc. Jpn **70** 1349(2000).
- 2) T. Jujo: J. Phys. Soc. Jpn **71** 888(2001).
- 3) M. I. Larkin, A. Kinkhabwala, Y. J. Uemura, Y. Sushko and G. Saito: Phys. Rev. B **64** 144514(2001).
- 4) C. Panagopoulos, J. R. Cooper, T. Xiang, Y. S. Wang and C. W. Chu: Phys. Rev. B **61** R3808 (2000).
- 5) T. Biggs, A. Klehe, J. Singleton, D. Bakker, J. Symington, P. Goddard, A. Ardavan, W. Hayes, J. Schlueter, T. Sasaki and M. Kurmoo: J. Phys. Condens. Matter **14** L495 (2002).
- 6) J. Caulfield, W. Lubczynski, F. L. Pratt, J. Singleton, D. Y. K. Ko, W. Hayes, M. Kurmoo. and P. Day: J. Phys. Condens. Mater **6** 2911 (1994).
- 7) A. Klehe, T. Tomita, J. S. Schilling, A. M. Kini, and J. A. Schlueter: Physica C **402** 17(2004).
- 8) T. Ishikawa, M. Maesato and G. Saito: Synth. Met. **133** 227(2003).
- 9) T. Mizutani, M. Tokumoto, T. Kinoshita, J.S. Brooks, Y. Uwatoko, O. Drozdova, K. Yakushi, I. Tamura, H. Kobayashi, T. Mangetsu, J. Yamada and K. Ishida : Synth. Met. **133** 229(2003).
- 10) J. Muller, M. Lang, F. Steglich, J.A. Schlueter, A.M. Kini, U. Geiser, J. Mohtasham, R.W. Winter, G.L. Gard, T. Sasaki and N. Toyota, Phys. Rev. B **61** 11739(2000).
- 11) H. Kino and H. Fukuyama: J. Phys. Soc. Jpn. **64** 2726 (1995).
- 12) H. Kino and H. Fukuyama: J. Phys. Soc. Jpn. **65** 2158 (1996).
- 13) T. Jujo, S. Koikegami and K. Yamada: J. Phys. Soc. Jpn. **68** 1331 (1999).
- 14) H. Kondo and T. Moriya: J. Phys. Soc. Jpn **67** 3695(1998).
- 15) H. Kondo and T. Moriya: J. Phys. Soc. Jpn **68** 3170(1999).
- 16) H. Kondo and T. Moriya: J. Phys. Soc. Jpn **73** 812(2004).
- 17) H. Kino and H. Kontani: J. Phys. Soc. Jpn **67** 3691(1998).
- 18) J. Schmalian: Phys. Rev. Lett. **81** 4232(1998).
- 19) T. Hotta: J. Phys. Soc. Jpn **63** 4126(1994).
- 20) G. M. Èliashberg: Sov. Phys. JETP **14** 886(1962).
- 21) T. Okabe: J. Phys. Soc. Jpn **67** 2792(1998).
- 22) H. Kontani, K. Kanki and K. Ueda Phys. Rev. B **59** 14723(1999).
- 23) M. Rahal, D. Chasseau, J. Gaultier, L. Ducasse, M. Kurmoo, and P. Day: Acta. Cryst. B **53** 159(1997).
- 24) K. Kanoda: Physica C **282-287** 299-302(1997).
- 25) A. Klehe, R. D. McDonald, A. F. Goncharov, V. V. Struzhkin, H. Mao, R. J. Hemley, T. Sasaki, W. Hayes, and J. Singleton: J. Phys. Condens. Mater **12** L247(2000).
- 26) K. Oshima, T. Mori, H. Inokuchi, H. Urayama, H. Yamoti and G. Saito: Phys. Rev. B **38** 938(1988).
- 27) A. Ugawa, G. Ojima, K. Yakushi, and H. Kuroda: Phys. Rev. B **38** 5122(1988).
- 28) A. Klehe, T. Biggs, C. A. Kuntscher, A. M. Kini, and J. A. Schlueter: cond-mat 0405445 (2004).
- 29) T. Jujo and K. Yamada: J. Phys. Soc. Jpn **68** 2198(1999).
- 30) T. Arai, K. Ichimura, K. Nomura, S. Takasaki, J. Yamada, S. Nakatsuji, and H. Anzai: Synth. Met. **120** 707(2001).
- 31) T. Arai, K. Ichimura, K. Nomura, S. Takasaki, J. Yamada, S. Nakatsuji, and H. Anzai: Solid State Commun. **116** 679(2000).
- 32) Y. Yanase, T. Jujo, and K. Yamada: J. Phys. Soc. Jpn **69** 3664(2000).

- 33) T. Takimoto and T. Moriya: Phys. Rev. B **66** 134516(2002).
- 34) H. Fukazawa and K. Yamada: J. Phys. Soc. Jpn **72** 2449(2003).